The International Journal of Advanced Manufacturing Technology (2020) 107:4357–4369
https://doi.org/10.1007/s00170-019-04709-8

ORIGINAL ARTICLE

Development and validation of a new friction model for cutting processes

Bingxiao Peng[1] · Thomas Bergs[1] · Daniel Schraknepper[1] · Thobias Smigielski[1] · Fritz Klocke[1]

Received: 17 September 2019 / Accepted: 12 November 2019 / Published online: 25 January 2020

Abstract
The friction model in the tool-chip interface has significant influences on predicting chip forms, cutting forces, and cutting tool temperatures, when simulating the chip formation using the finite element method. In this paper, the friction behavior in the tool-chip interface was investigated experimentally and numerically under cutting conditions. The friction tests were performed with different workpiece materials (AISI 1045 and Direct Aged Inconel 718) in combination with uncoated and coated cemented carbide cutting tools. Various process normal forces were applied to achieve different contact pressures. The experimental results showed strong influences of relative speeds, contact pressures, and contact temperatures on apparent friction coefficients. In addition, an advanced friction model was proposed and validated with 3D FE-simulations of the friction test.

Keywords Friction model · Cutting process · Cemented carbides · FEM

1 Introduction

With the development of computational technology, modeling and simulation of cutting processes show the growing importance and potential in industry. The material constitutive law and the friction model at the tool-chip interface are the key factors for precise cutting simulations using the finite element method (FEM) [4]. According to Arrazola and Özel, the friction model has a significant influence on predicting cutting forces, chip forms, contact lengths, and cutting temperatures for FEM cutting simulations [3, 25]. Arrazola also expressed that an insufficient friction model could be a reason for the underestimation of the cutting normal force [5]. Recent studies also show that the use of a constant Coulomb friction model is not sufficient for the cutting simulation. In cutting processes, high strains, strain rates, and temperatures occur in primary and secondary shear zone [17, 24]. These extreme conditions make the investigations of the friction behavior at the tool-chip interface particularly important.

✉ Bingxiao Peng
b.peng@wzl.rwth-aachen.de

[1] Laboratory for Machine Tools and Production Engineering (WZL) of RWTH Aachen University, Campus-Boulevard 30, 52074 Aachen, Germany

Melkote et al. reviewed recent advances in the identification of friction behaviors for cutting simulations [20]. Different friction mechanisms and experimental methods under cutting conditions have been discussed. According to their work, developing experimental methods to separate the adhesion and deformation components in friction behavior is necessary for future researches. Furthermore, a comparative assessment of the accuracy of existing friction models is expected.

To describe the contact behavior at the tool-chip interface, also known as the secondary deformation zone, various friction models have been investigated. A constant coefficient of friction according to the Coulomb law can be calculated by Merchant analysis [21].

$$\mu = \frac{F_f + F_c \times \tan\gamma}{F_c - F_f \times \tan\gamma} \tag{1}$$

This friction model is mainly used in engineering, because the apparent friction coefficient can be easily calculated with respect to the cutting force F_c, the feed force F_f, and the rake angle γ (Eq. 1). Moreover, the Merchant analysis assumes that the cutting tool edge is ideally sharp. The influence of the ploughing effect is therefore neglected in the Merchant analysis. Abrecht [1] proposed a modified calculation of friction coefficients that

took ploughing cutting force P_c and ploughing feed force P_f into account (Eq. 2).

$$\mu = \frac{(F_f - P_f) + (F_c - P_c) \times \tan\gamma}{(F_c - P_c) - (F_f - P_f) \times \tan\gamma} \tag{2}$$

An analytical investigation of friction shows that the apparent friction coefficient consists of the adhesion μ_a and deformation μ_m terms [15] (Eq.3). The adhesion term can be derived in relation to the limited shear stress τ_f, which is depending on the equivalent flow stress $\overline{\sigma}$. The deformation term of the rake face friction in orthogonal cutting can be derived as a function of shear angle Φ and rake angle γ.

$$\mu = \mu_a + \mu_m = \frac{\tau_f}{\overline{\sigma}} + \arctan(\frac{\pi}{4} - \Phi + \gamma) \tag{3}$$

Zhou [30] proposed an analytical friction model that considers the sticking, transition, and sliding friction at the tool-chip interface. The proposed model calculates the global and local friction coefficient by inverse determination of the shear stress in the secondary shear zone based on a thermo-mechanical analysis. The author validated the model by comparing the experimental data and the data from the literature. However, the proposed analytical model was based on various assumptions such as the chip compression ratio, the shear angle, and the heat partition coefficient, which also depend on cutting parameters. It is a general disadvantage of analytical friction models.

Empirical models have also been investigated in recent years. Moufki et al. [22] and Puls et al. [26] proposed the temperature-dependent friction models at the tool-chip interface based on the thermal softening theory (Eq. 4). This friction model indicates that the apparent friction coefficient stays a constant value of μ_0 up to a temperature of T_r and then decreases with the increasing of the temperature due the thermal softening effect in relation to the melting temperature T_m and the power m_r. Moufki et al. determined analytically the mean temperature and the apparent friction coefficient at the tool-chip interface. Puls et al. measured the temperature and the apparent friction coefficient on a friction test bench under cutting conditions. It should be noted that the temperature-dependent friction model was proposed under the assumption that the effects of speeds and pressures act only on contact temperatures. However, the friction behavior under cutting conditions is more complicated.

$$\mu = \mu_0 \times \left(1 - \left(\frac{T - T_r}{T_m - T_r}\right)^{m_r}\right) \tag{4}$$

Zemzemi et al. [29] and Bonnet et al. [8] investigated the apparent friction coefficients with a specific designed tribometer based on a modified pin-on-ring system. They investigated the friction behavior depending on the sliding speed for the workpiece materials AISI 4142 and AISI 316L with different carbides under dry cutting conditions. A friction model as a function of the sliding speed v_s was proposed, as shown in Eq. 5. The coefficients c_1 and c_2 were determined by means of experimental and numerical investigations. The authors tried to separate the adhesion and plastic friction when modeling the tool-chip interface. Based on their studies, Rech et al. [27] investigated the friction behavior for different workpiece materials under dry and wet cutting conditions. A similar work was performed by Smolenicki et al. [28] on an in-process tribometer in orthogonal turning process. Based on empirical data, the authors introduced also sliding speed-dependent friction models for different workpiece materials and cutting tool materials. However, the introduced friction models were not implemented and validated in FEM simulations. In addition, the influence of temperatures and pressures was not investigated.

$$\mu = c_1 \times (v_s)^{-c_2} \tag{5}$$

Furthermore, Brocail et al. [9] have experimentally and numerically studied the influence of temperatures and pressures on apparent friction coefficients. The authors controlled the initial workpiece temperature, the workpiece penetration, and the sliding speed to achieve different temperatures and contact pressures under cutting conditions. The contact pressure and temperature were determined by an inverse numerical approach. A friction model was then proposed as a function of the normal stress σ, sliding speed v_s, and contact temperature T (Eq. 6). The coefficients for the friction model c_1, c_2, and c_3 were determined experimentally and numerically. The friction model was not implemented into the FE model and was therefore not validated. A similar friction model was developed by Klocke et al. [19] in sheet metal forming simulations. The proposed friction model was implemented and validated in the FEM forming simulation. It should be noted that the working conditions in sheet forming were significant different from the cutting conditions with respect to the contact pressure, the temperature, and the sliding speed.

$$\mu = c_1 \times (v_s)^{c_2} \times (T)^{c_3} \times (\sigma)^{c_4} \tag{6}$$

In this paper, the friction behavior of the workpiece materials Direct Aged Inconel 718 (DA718) and AISI1045 with different cemented carbides was experimentally investigated. Modified friction tests were performed on the test bench presented by Puls et al. [26]. Different relative speeds and process normal forces were applied to study the influence of the normal stress on the friction behavior. The investigated variables are shown by a cause-and-effect diagram in Fig. 1. The friction model based on Eq. 6 was then determined as a function of the relative speed, temperature and normal stress. In addition, the determined friction model has been implemented into a 3D CEL-based

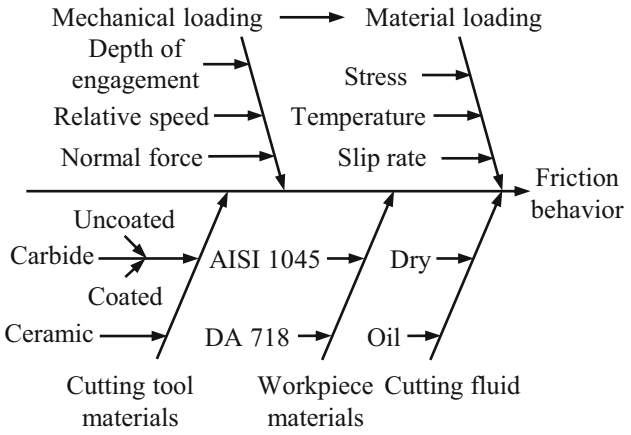

Fig. 1 Cause-and-effect diagram for investigating the friction behavior according to Ishikawa [16]

FE model for the friction tests and validated with respect to the apparent friction coefficient.

2 Experimental investigation

2.1 Experimental setup

A friction test bench has been designed on a vertical broaching machine tool RASX 8 × 2200 × 600 M/CNC from Forst Technologie GmbH, as shown in Fig. 2. The broaching machine has a stoke length of 2200 mm and a maximum cutting speed of 150 m/min. For the cutting speeds lower than 30 m/min, the maximum broaching force is 80 kN. For the cutting speed from 30 to 150 m/min, the maximum broaching force is 20 kN. The basic setup of the friction test is the same as the one developed by Puls et al. [26]. Workpieces in sheet geometry were clamped by a holder mounted on the linear machine tool drive. The typical C-type turning insert was placed in a customized tool holder. A customized tool holder was mounted on the Kistler dynamometer Z21289 which can measure the process forces F_z and F_y in friction tests.

Instead of studying the friction behavior between the original rake face of turning insert tools and the workpiece in orthogonal cutting, the setup enables the contact between the original flank face and the workpiece with a linear motion v_r. The workpiece tool contact happens between the workpiece and original flank face, which can also be considered as a ploughing process with a large negative rake angle. The friction behavior was investigated by this analogy test bench and experimental design, in which the chip formation is suppressed. Although there is no material separation in the analogy friction tests, the friction behavior was investigated with respect to the material loading including high strains, strain rates, and high temperatures under cutting conditions. The chip breaker on the rake face will not affect the experimental results. The basic geometry of the CNMG120408 insert tool is normed, which is characterized by the corner radius $r_\epsilon = 0.8\,\mu$m and the shape angle of 80°. The 3D FEM friction simulation was also established based on the two geometrical factors. In addition, the contact interface can be characterized and adjusted by the tool inclination angle $\alpha = 9°$ and the depth of engagement t.

Apart from the process forces, the contact temperature T_m was measured by a two-color-pyrometer fiber during

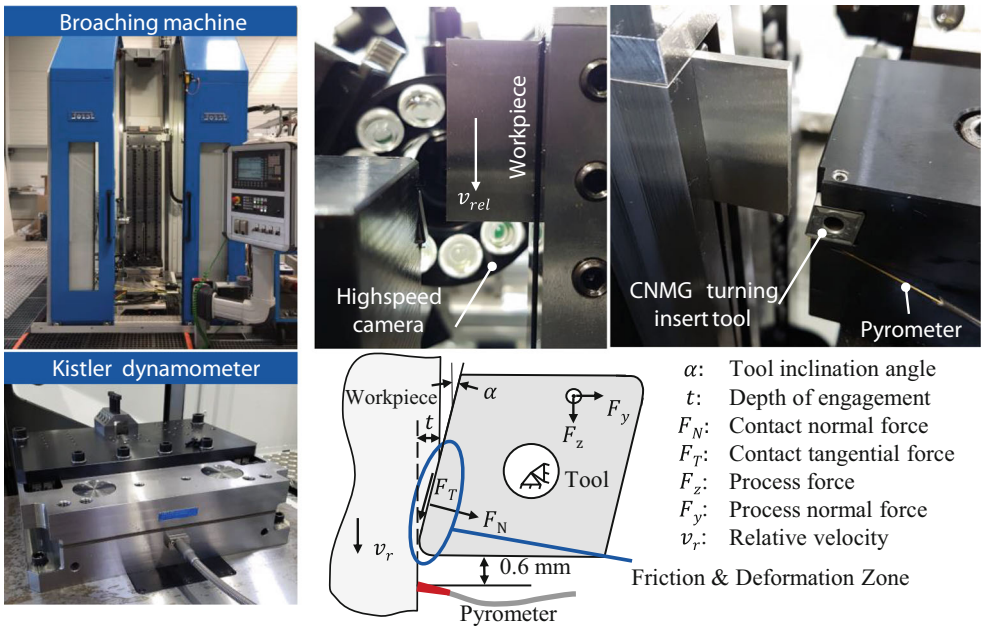

Fig. 2 Experimental setup

friction tests. The measurement spot on the workpiece was located 0.6 mm under the cutting insert. The use of the pyrometer is independent of emissivity variations, and it is suitable for transient processes due to its short response time.

In comparison to the previous friction tests with a constant depth of engagement, modified friction tests were conducted in this study under various defined process normal forces of F_y = 500, 2000, 4000, and 6000 N. The defined process normal force was realized as shown in Fig. 3. Before the workpiece moved linearly with a relative speed v_r, the C-type insert was penetrated into the workpiece with quasi-static movement to achieve a defined force F_y. The force was measured and controlled by the Kistler dynamometer. After reaching the defined force, the position of the insert was recorded and the insert was moved out. Although the process normal forces in friction tests were always slightly smaller than those in quasi-static loading due to compensation of the friction force, the research range of the normal force can be controlled by using this method. In addition, controlling the measurable process normal forces is better than controlling the depth of engagement, since the depth of engagement has an unmeasurable change due to the deformation of the insert tool in friction tests. By means of this experimental design, the influence of process normal forces and contact pressures on the friction behavior can be studied. With the following equations, the friction coefficient can be calculated depending on the process force F_z, process normal F_y, and the tool inclination angle α, as shown in Fig. 2.

$$\mu = \frac{F_T}{F_N} = \frac{F_z \times \cos\alpha - F_y \times \sin\alpha}{F_y \times \cos\alpha + F_z \times \sin\alpha} \tag{7}$$

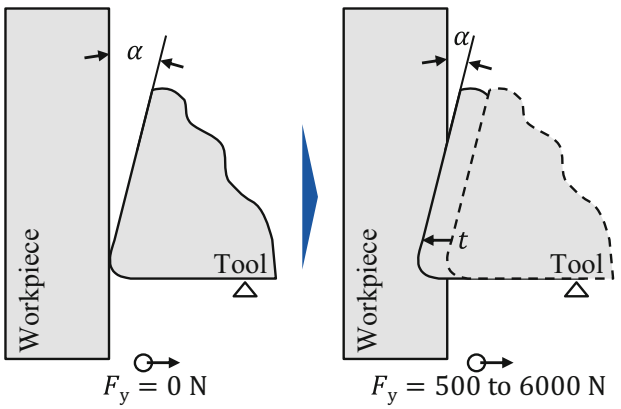

Fig. 3 Experimental conditions controlled by the process normal force (F_y)

Table 1 Characterization of workpiece materials

Material	Heat treatment	Density	Yield stress	Hardness
–	–	kg/m^3	MPa	–
AISI1045	Normalized	7821	476	HB 199
DA718	Direct aging	8190	1260	HV30 470

2.2 Cutting tools and workpiece materials

From the point of view of friction mechanisms, the friction behavior is a combination of the adhesion and deformation in the contact zone. The deformation is usually dependent on workpiece materials and process parameters. The adhesion is related to the contact pair as well as the contact pressure and temperature. Since the dominance of the two mechanisms is still unclear in cutting processes, it is worth investigating the effects of workpiece materials and cutting tool materials on the friction behavior. In this study, the normalized carbon steel AISI1045 and the direct aged Inconel 718 (DA718) were used. The workpiece materials were selected according to their thermal and mechanical properties, as shown in Table 1. Figure 4 shows their microstructures.The used workpiece had a thickness of b = 1.5 mm.

In comparison to AISI1045, DA718 belongs to the group hard-to-cut materials due to its high-temperature resistance, low thermal conductivity, and tendency to strain hardening, which leads to extremely high mechanical and thermal load on the cutting edge during machining. Various cutting tools were used as listed in Table 2. Cutting tool materials including the uncoated carbides WC-6Co (6 wt% Co) and WC-15Co (15 wt% Co), and the coated carbide + TiAlN (PVD) and the whisker-reinforced alumina ceramic Al_2O_3+SiC-Whisker were used to investigate the influence of cutting tool materials. Since the contact occurs only one the original flank face, C-type cutting tool inserts with different cutting tool materials were chosen although they have different chip breakers, as shown in Table 2.

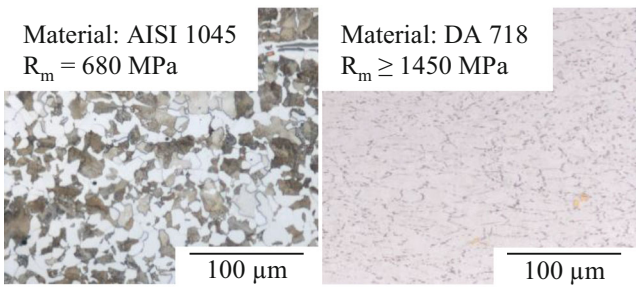

Fig. 4 Microstructure of investigated materials

Table 2 Characterization of cutting tool inserts

Type –	Manufact. –	Material code –	Coating –	Hardness (HV30)	Corner radius r_ϵ / μm
CNMG120408-SM	Sandvik	H13A (WC-6Co)	–	1600	0.8
CNMG120408	Extramet	EMT815 (WC-15Co)	–	1120	0.8
CNMG120408-23	Sandvik	GC1005 (coated WC-Co)	TiAlN (PVD)	1614	0.8
CNMG120708-T	Greenleaf	WG-300 (Al_2O_3+SiC-Whisker)	–	2168	0.8

2.3 Experimental results

With the above experimental setup and design, friction tests were performed under different process normal forces F_y, relative speeds v_r, and material combinations, as shown in Table 3. Figure 5 shows the signals of measured process forces F_z, F_y, and temperature T_m on the workpiece surface. Apparent friction coefficients μ were then calculated according to the Eq. 7. The measured process normal force F_y is slightly different from the force in static state due to the contribution of the friction force and the dynamic material behavior. For a process normal force $F_y = 2000\,\text{N}$, the apparent friction coefficient for $v_r = 20\,\text{m/min}$ is higher than for $v_r = 100\,\text{m/min}$ ($\mu = 0.24 > 0.1$). Many researches indicated that the material thermal softening effect is the main cause or the only reason for the reduction of the friction coefficient induced by the higher relative speed [22, 23, 26, 27]. However, if we compare the μ at different process normal forces, it can be noticed that the friction coefficient at $F_y = 6000\,\text{N}$ ($\mu = 0.16$) is higher than it at $F_y = 2000\,\text{N}$ ($\mu = 0.1$), although the temperature is also higher ($T = 679 > 456\,^\circ\text{C}$). This phenomenon indicates that the temperature might not be the only physical variable that affects the friction behavior.

Figure 6 shows a detailed and systematic analysis in terms of contact tangential forces F_T, contact normal forces F_N, and measured contact temperatures T_m in the steady state. Process forces are reflections of the friction behavior. On the one hand, the contact normal force decreased slightly with the increase of the relative speed v_r. On the other hand, the contact tangential force decreased obviously with the v_r for all material combinations and process normal forces.

It is generally accepted that the apparent friction coefficient in cutting processes depends on cutting speeds, undeformed chip thicknesses, and contact pairs. The apparent friction coefficient μ, calculated by the Eq. 7, decreased gradually with the increase of the relative speed in dry conditions, which has also been observed in other researches [10, 13, 27]. For the material combination of DA718 and WC-15Co, the apparent friction coefficient μ decreased from 0.36 to 0.16 when v_r increased from 20 to 100 m/min under a process normal force $F_y = 6000\,\text{N}$. It is also noted that μ is also influenced by F_y. For the same material combination of DA718 and WC-15Co, μ for $F_y = 6000\,\text{N}$ is generally 0.11 higher than for $F_y = 2000\,\text{N}$. Furthermore, the contact temperature increased with the relative speed. For the contact pair DA718 and WC-15Co, the contact temperature increased from 552 to 679 °C when v_r increased from 20 to 100 m/min. This phenomenon can be explained by the increase of the total dissipated process power due to the higher strain rate in the contact zone. Earlier researches [22, 26, 27] explained the decrease of friction coefficients using the thermal softening theory. This theory assumes that relative speeds and contact pressures affect only the contact temperature, which influences the friction behavior by softening the material strength indirectly, as discussed in Section 1.

By presenting the apparent friction coefficients μ as a function of the measured contact temperature T_m, interesting results can be observed. For all material combinations, the decrease trend of the friction coefficient (μ) with the increase of the contact temperature T_m was observed under the same process normal force. However, the same friction coefficient can be achieved when contact

Table 3 Experimental plan of the friction test

Workpiece material –	Cutting tool material –	Process normal force F_y / N	Relative speed v_r / m/min	Lubricant –
DA718	WC-15Co	500/2000/4000/6000	20/40/60/100	Dry
DA718	WC-Co + TiAlN	500/2000/4000/6000		Dry
DA718	Al_2O_3+SiC-Whisker	4000		Dry
DA718	WC-15Co	2000/4000		Castrol Variocut B9
AISI1045	WC-6Co	500/2000/4000/6000		Dry

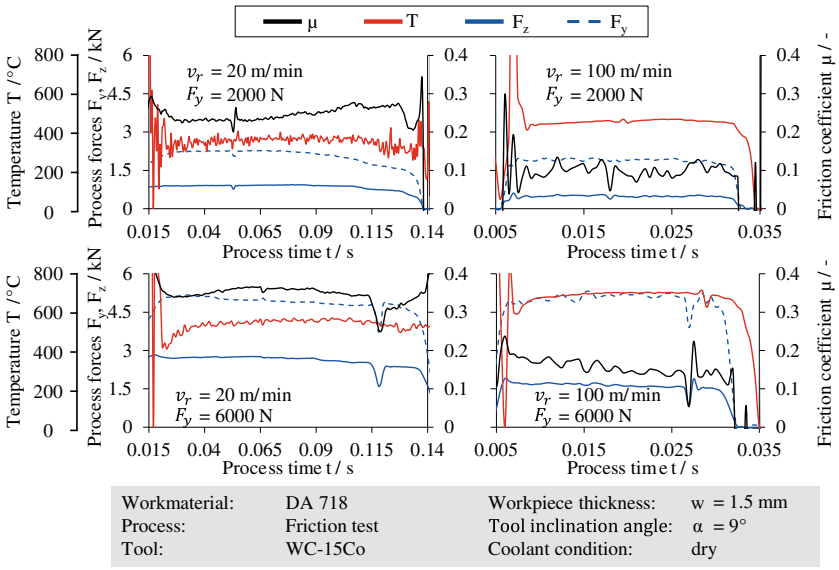

Fig. 5 Measurement of process forces and temperatures in the friction test

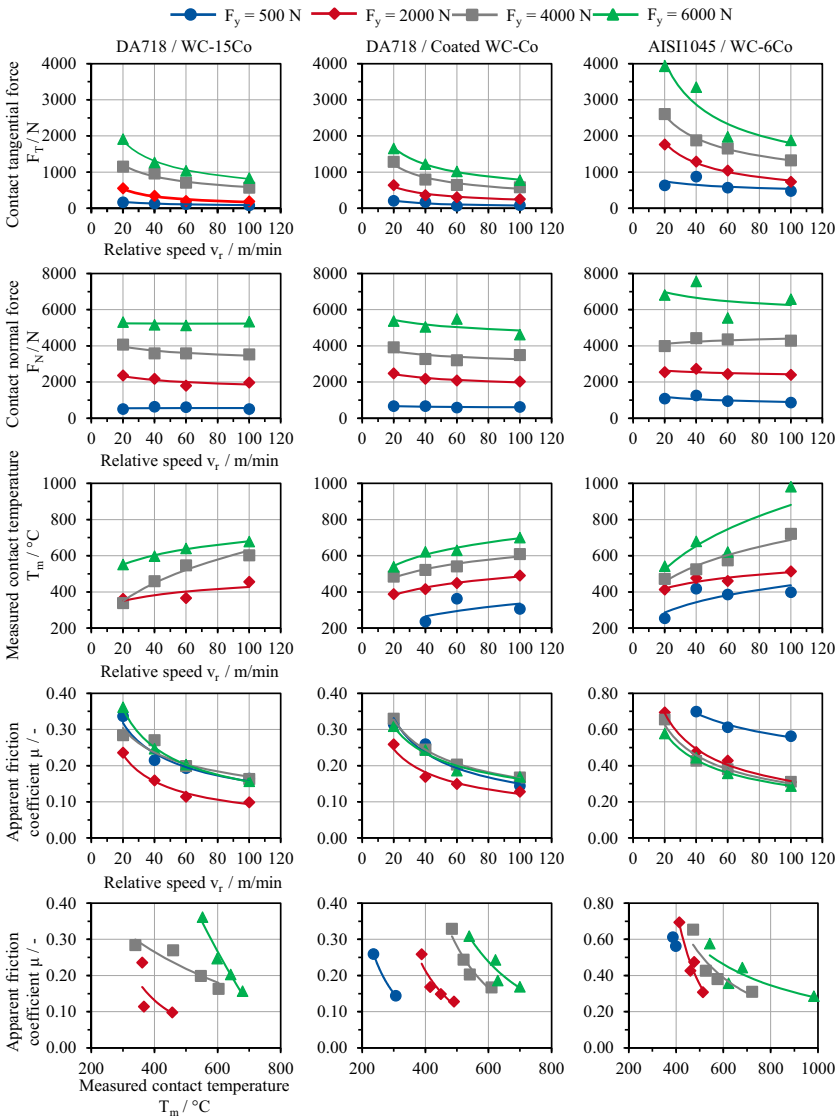

Fig. 6 The contact forces F_T / F_N, measured contact temperature T_m, and apparent friction coefficient μ with respect to the material combination and process normal force F_y in dry conditions

temperatures and process normal forces increase together. For examples, for the material combination of DA718 and coated WC-Co, a similar friction coefficient $\mu = 0.24 - 0.26$ can be observed at $T = 236\,°C/F_y = 500\,\text{N}$, $T = 388\,°C/F_y = 2000\,\text{N}$, $T = 522\,°C/F_y = 4000\,\text{N}$, and $T = 623\,°C/F_y = 6000\,\text{N}$. For the workpiece made of AISI 1045, the friction coefficient is generally higher than DA718. In addition, the friction coefficient at $F_y = 500\,\text{N}$ is significantly higher than at other process normal forces. The explanation for these differences between AISI1045 and DA718 is the change in friction mechanisms, in particular, the deformation term due to workpiece material properties.

It can be concluded that the use of temperature as the only physical parameter to describe the friction behavior is not sufficient. The relative speed and the process normal force can influence the friction behavior directly instead of via the contact temperature. According to the principle of dynamics, while increased temperature can enhance the heat movement capacity of the moving objects, it also increases the distance of molecule due to thermal expansion. After the relaxation process of high polymer, its physical properties such as visco-plasticity and thermodynamics nature will also alter significantly. In general, when environment temperature increases, the material's surface friction coefficient will undergo certain changes, changing proportion however will vary from material to material. Since contact temperatures in this investigation cannot be separated from relative speeds and process normal forces, no direct conclusion can be drawn about the temperature. These phenomena with respect to workpiece materials, contact temperatures, relative speeds, and process normal forces can be traced back to the friction mechanisms.

After friction tests, the contact surfaces of cutting tool inserts captured by the digital microscope VHX-5000, as shown in Fig. 7. Workpiece material adhering to the tool material can be identified. With the increase of F_y, more workpiece material was adhered to the tool material. This phenomenon can be classified as the adhesion friction mechanisms.

The friction behavior reacts differently in terms of the relative speed. In order to investigate the friction mechanism, the element analysis was performed on the contact surface by energy-dispersive X-ray spectroscopy (EDX), as shown in Fig. 8. Adhering effect of the nickel-based alloy DA718 can be identified by the element Ni. The coating TiAlN was identified by the element Ti. The subtract of the cemented carbide was identified by the element W. For the material combination of DA718 and uncoated cemented carbide, both adhesion and sliding exist at a higher speed $v_r = 100\,\text{m/min}$, while adhesion dominated the friction mechanisms at a lower speed $v_r = 20\,\text{m/min}$.

For the material combination of DA718 and coated cemented carbide, the substrate can be identified on the contact area because the coating was chipped off at both speeds. Meanwhile, the material at the workpiece boundary layer has reached the limited shear stress induced by the material deformation. Due to the property of coating, the boundary layer tends to separate rather than adhere. At a lower speed, the trend towards separations with coated carbide is more obvious.

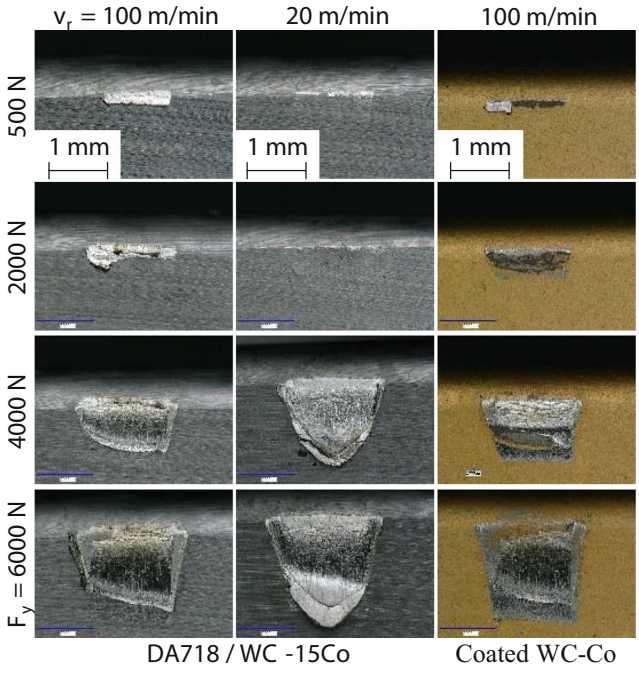

Fig. 7 Contact areas under different process normal forces and material combinations

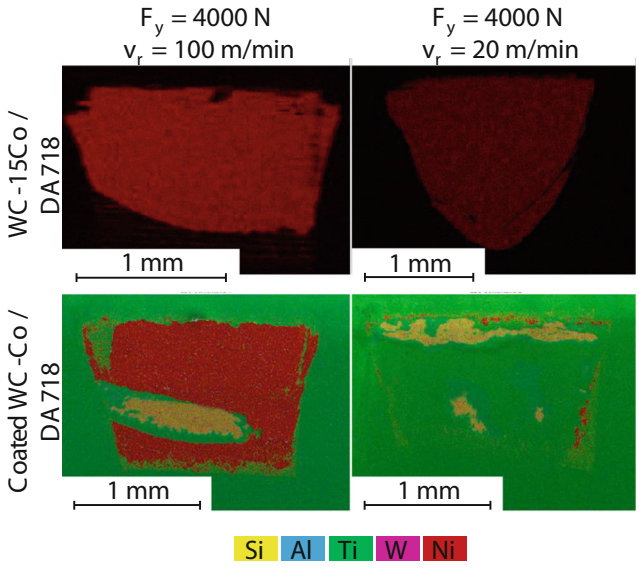

Fig. 8 Element distribution by EDX mapping on the contact area

2.3.1 Influence of cutting tool materials and cutting fluid

Figure 9 shows the SEM and EDX analysis of the contact surfaces for different cutting tool materials after friction tests. Although the workpiece material appeared on each material combination, they behaved differently. For the uncoated cemented carbide, the adhered workpiece material spreads over the contact area except the sliding part. From the SEM analysis, the WC-Co, the coating layer and the adhered material DA718 can be well observed in the transition zone, where the coating together with the adhesive material chipped off due to high pressure and mechanical scratching by hard carbides such as TiC in DA718. In the case of whisker-reinforced ceramics, the adhesion distributed overall, except at the tool corner. Based on the EDX and SEM analysis, the material adhering to the ceramic is smoother and has a lower material shear effect than coated/uncoated WC-Co, indicating less material deformation in the contact zone. This phenomenon correlates also with the wear mechanism when machining nickel-based alloys with cemented carbides and whisker-reinforced ceramics. The material shear effect at the boundary layer reflects the friction coefficient. Figure 10 shows the influence of cutting tool materials on friction coefficients under dry conditions. The friction coefficients for uncoated and coated cemented carbides are almost identical despite their different adhesion trends. The friction coefficients for ceramic is however slightly lower than carbides due to its less material deformation. It can be concluded that the workpiece deformation is the main friction mechanisms in comparison to the adhesion term.

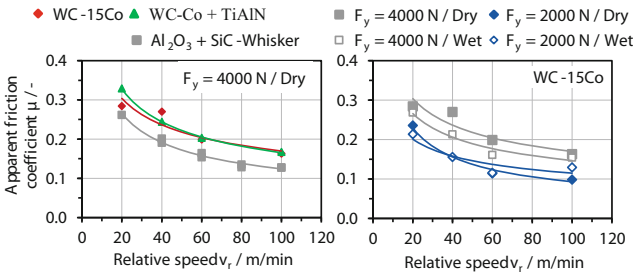

Fig. 10 Influence of cutting tool materials and cutting fluid on the friction behavior with workpiece material DA 718

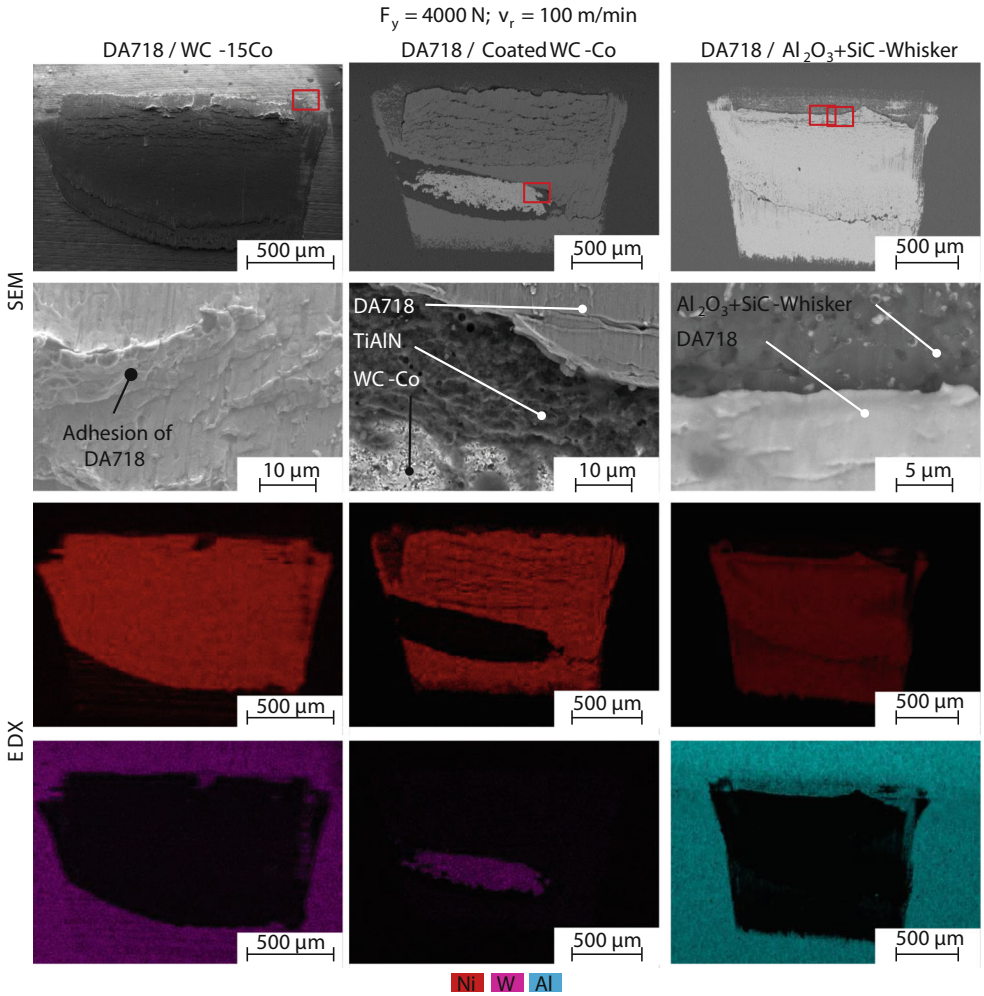

Fig. 9 SEM and EDX analysis of the contact surface in test tools at $F_y = 4000\,\mathrm{N}$ and $v_r = 100\,\mathrm{m/min}$

Furthermore, the influence of the cutting fluid was investigated under $F_y = 2000\,\text{N}$ and 4000 N, as shown in Fig. 10. Castrol Variocut B9 oil developed for high-performance broaching in aerospace industry, was used as the flood lubricant. In contrast to friction tests with CO_2 and emulsion [27], the use of the cutting fluid showed only a limited effect on the friction coefficient at lower process normal force $F_y = 2000\,\text{N}$, while the μ with cutting fluid is generally 0.05 less than dry tests under $F_y = 4000\,\text{N}$.

3 Identification and validation of a new friction model

According to the experimental investigation, the apparent friction coefficient decreased with increasing the relative speed v_r and the contact temperature T_m. It must be noted that the change of the contact temperature was induced by different relative speeds ($v_r = 20 - 100\,\text{m/min}$) and process normal forces ($F_y = 500 - 6000\,\text{N}$). The experimental results indicated that a pure temperature-dependent friction model is not sufficient to describe the friction behavior in cutting conditions. The relative speed and the process normal force affect the friction behavior not only via the induced temperature. However, the depth of engagement is not a physical variable that cannot be applied to a friction model for further FEM simulations. As discussed, the workpiece deformation is one of the major friction mechanisms which can be influenced by temperatures, strains, and strain rates. From this point of view, the process normal force and the relative speed might affect the friction behavior by changing the workpiece deformation. Overall, the friction behavior will be modeled as a function of speed, temperature, and pressure in this section.

An inverse approach to determine the depth of engagement t was performed by comparing the experimental and simulative results, as shown in Fig. 11. Due to the deformation of the insert tool in friction tests, the depth of engagement t was deviating from the record and cannot be predefined directly for the corresponding FE model of each friction test. Since the contact area was difficult to be measured due to the different friction mechanisms, as shown in Fig. 7, the average contact pressure cannot be derived from the experimental contact area and contact normal force. Determining the depth of engagement t was becoming a necessary and challenging step to analyze the apparent friction coefficient.

In this approach, a 3D FEM model with ABAQUS explicit for the friction tests was established based on the coupled Eulerian–Lagrangian (CEL) formulation [26]. The workpiece was modeled as an Eulerian domain with the 3D element EC3D8RT and a minimum element size of 0.05 mm. The tool was defined as a Lagrangian rigid body

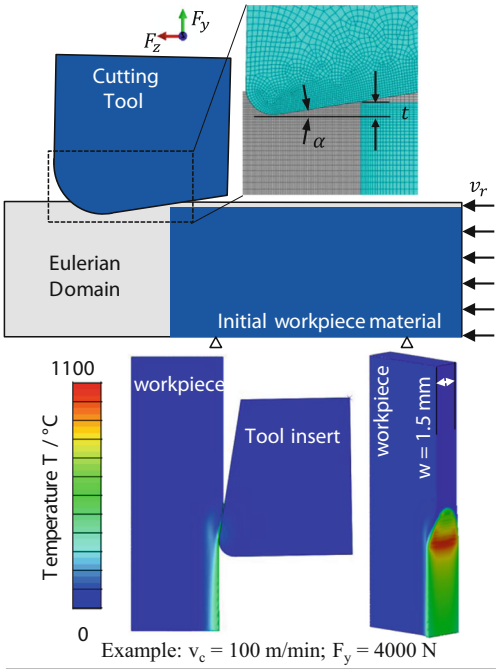

Example: $v_c = 100$ m/min; $F_y = 4000$ N

	t / mm	F_T / N	F_N / N	μ / -	CF
Exp	0.22	576	3531	0.16	0
Sim_1	0.24	887	5856	0.15	0.80
Sim_2	0.21	797	5283	0.15	0.45
Sim_3	0.18	709	4683	0.15	0.19
Sim_4	0.15	618	4109	0.15	0.05
Sim_5	**0.12**	**527**	**3550**	**0.15**	**0.01**

Fig. 11 A numerical approach to determine the depth of engagement t as well as the friction model

with the element C3D8RT and a minimum element size of 0.05 mm. In addition, a mass scaling factor of 1000 was implemented to achieve a stable time increment more than $\Delta t = 10^{-7}\,\text{s}$, and thus to accelerate the simulation. The depth of engagement t, the tool inclination angle α, and the relative speed v_r were defined corresponding to the test conditions of the friction tests. The parameters of the Johnson–Cook (JC) material model, as shown in Eq. 8, and the other material properties for DA 718 and WC-15Co were obtained from previous work [18]. The JC material model describes empirical dependencies of the flow stress. It consists of a strain ϵ term, a strain rate $\dot{\epsilon}$ term, and a temperature T term. According to the JC constitutive model, the equivalent flow stress (σ_{JC}) can be calculated with the parameters A, B, n, C, and m. The parameters of JC material model are listed in Table 4

$$\sigma_{\text{JC}} = \left(A + B \times \epsilon^n\right) \times \left(1 + C \times \ln \frac{\times \epsilon}{\times \epsilon_0}\right) \times \left(1 - \left(\frac{T - T_0}{T_m - T_0}\right)^m\right) \tag{8}$$

The tool-workpiece contact interface between the Lagrangian element (the tool) and the Eulerian element

Table 4 Parameters for the Johnson–Cook material constitutive model of DA718 [18]

A /MPa	B /MPa	n -	C -	m -	$\dot{\epsilon}_0$ /s^{-1}	T_m /°C	T_0 /°C
1262	1354	0.5	0.006	1.08	0.001	1340	25

(the workpiece material) was defined by a contact interaction, which consists of a constant friction coefficient and a penalty contact formulation. The constant friction coefficient $\mu(v_r, F_y)$ was defined at a certain relative speed and process normal force based on the experimental tests. Furthermore, a constant heat contact conductance $h_c = 10,000\,\mathrm{mW/mm^2K}$ was utilized in order to achieve the steady state of heat transfer between the workpiece and the tool in a short time [11]. Starting from an initial depth of engagement, the depth of engagement was changed in the FEM model iteratively until the percentage square error CF according to the loss function Eq. 9 satisfied, which takes into account the contact normal force F_N, the contact tangential force F_T, and the apparent friction coefficient μ. Figure 11 also shows the inverse approach to determine the depth of engagement $t = 0.12\,\mathrm{mm}$ for the case $v_r = 100\,\mathrm{m/min}$ and $F_y = 4000\,\mathrm{N}$.

$$\mathrm{CF} = \left(\frac{\mu_{\mathrm{sim}}-\mu_{\mathrm{exp}}}{\mu_{\mathrm{exp}}}\right)^2 + \left(\frac{F_{T,\mathrm{sim}}-F_{T,\mathrm{exp}}}{F_{T,\mathrm{exp}}}\right)^2 + \left(\frac{F_{N,\mathrm{sim}}-F_{N,\mathrm{exp}}}{F_{N,\mathrm{exp}}}\right)^2 < 0.05 \tag{9}$$

The numerical inverse approach was performed for each relative speed and process normal force to determine the depth of engagement. Figure 12 shows the apparent friction coefficient μ, the contact temperature T, the contact pressure p, and the tangential contact force F_T as a function of the relative speed v_r and depth of engagement t from the numerical approach and the corresponding experimental results.

The inverse numerical approach has a good agreement with the experimental results, as shown in Eq. 10. The friction coefficient increased with increasing the engagement depth and decreasing the relative speed. The mean contact pressure was then calculated with respect to the contact area and contact normal force which can be obtained directly from the FEM simulation.

$$\begin{aligned}\mu_{\mathrm{sim}} &= 2.0738 \times t^{0.3266} \times v_r{}^{-0.4502}\\ \mu_{\mathrm{exp}} &= 1.9978 \times t^{0.2618} \times v_r{}^{-0.4488}\end{aligned} \tag{10}$$

By means of the numerical approach, a friction model for the workpiece material DA 718 and the uncoated cemented carbide WC-15Co was derived as a function of the relative

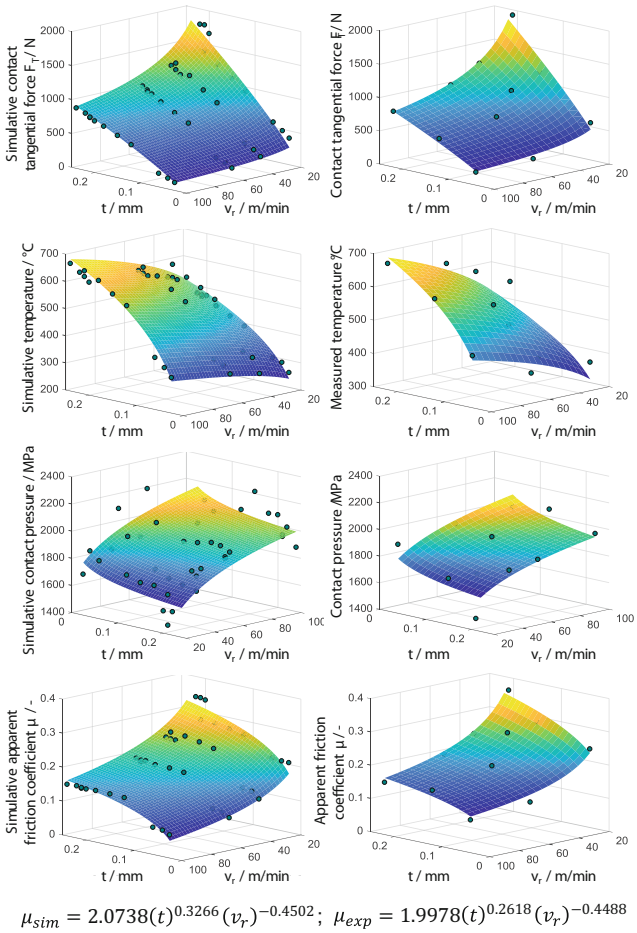

Fig. 12 Apparent friction coefficient as a function of the depth of engagement t and the relative speed v_r

speed v_r (m/min), the measured temperature T_m (°C), and the mean contact pressure p_m (MPa) from the experimental v_r and T_m and numerical p_m data, as shown in Eq. 11.

$$\mu = 0.5085 \times \left(\frac{v_r}{40}\right)^{-0.546} \times \left(\frac{T_m}{1340}\right)^{0.2204} \times \left(\frac{p_m}{1000}\right)^{-0.5474} \tag{11}$$

The coefficients of the proposed friction model were calculated by solving a least square nonlinear equation with the Levenverg–Marquardt optimization method. As expected, the apparent friction coefficient decreased with increasing the relative speed and the contact pressure. A proportional relationship between the friction coefficient and the temperature was identified by the proposed friction model. As discussed in Section 1, the softening effect was observed by many researchers at higher temperatures induced by high speed and high engagement, which results in a lower friction coefficient. However, this conclusion was based on the assumption that the relative speed and

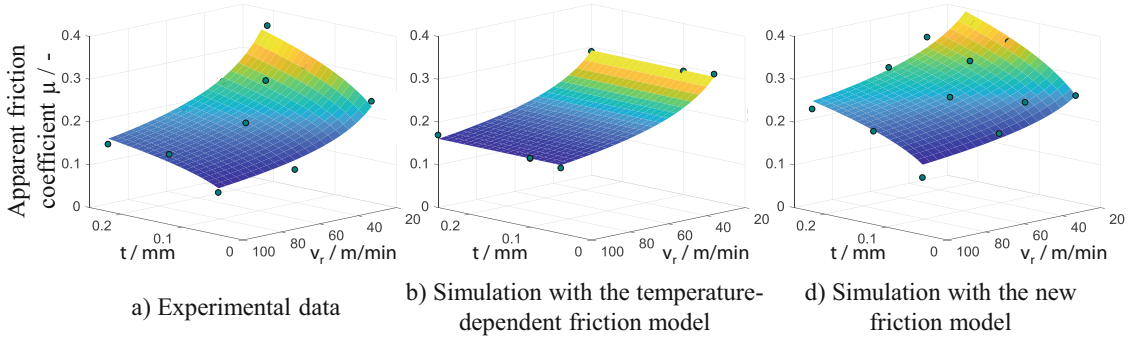

Fig. 13 Validation and comparison of the new friction model with the temperature-dependent friction model

the contact pressure only affects the temperature. As we know, the apparent friction coefficient can be estimated by summing the adhesion and deformation terms. Higher temperatures reduce the limited shear stress due to thermal softening. However, the deformation term cannot be easily determined by the temperature. The material movement under the sticking contact surface can be assumed to be liquid. The phenomena can be explained with respect to the internal friction, which acts as the damping capacity [6]. According to the research by Fukuhara and Sanpei [14], the internal friction of Inconel 718 increased with increasing temperatures in elastic deformation. Although the limit shear stress decreases with increasing the temperature, more energy is required due to the deformation term. A similar phenomenon was also identified by Brocail et al. [9] under different controlled temperatures. In their study, a higher temperature leads to a higher friction coefficient. Similar results regarding to the friction coefficients were obtained by Bobzin et al. [7]. According to their experimental investigation, the friction of coefficient between uncoated substrate AISI D2 and AISI 5115 increased at a higher temperature. For better understanding the friction behavior related to the temperature, it is necessary and worth to find a way to study the influence of the temperature separately under cutting conditions.

The proposed friction model was then implemented into the FEM friction model under different relative speeds and depth of engagements determined by the numerical approach. Figure 13 shows the apparent friction coefficient from the experiments and the simulations with the proposed friction model as well as with the temperature-dependent friction model from previous work [18]. The previous friction model is not able to model the influence of the depth of the engagement on the friction coefficient. On the other hand, the proposed friction model has successfully described the influence of the t and the v_r. The pyrometer could not access to the contact interface during the process, because the tool-workpiece interface was closed due to the high contact pressure. In the case of placing a pyrometer or thermocouple in a drilling hole,

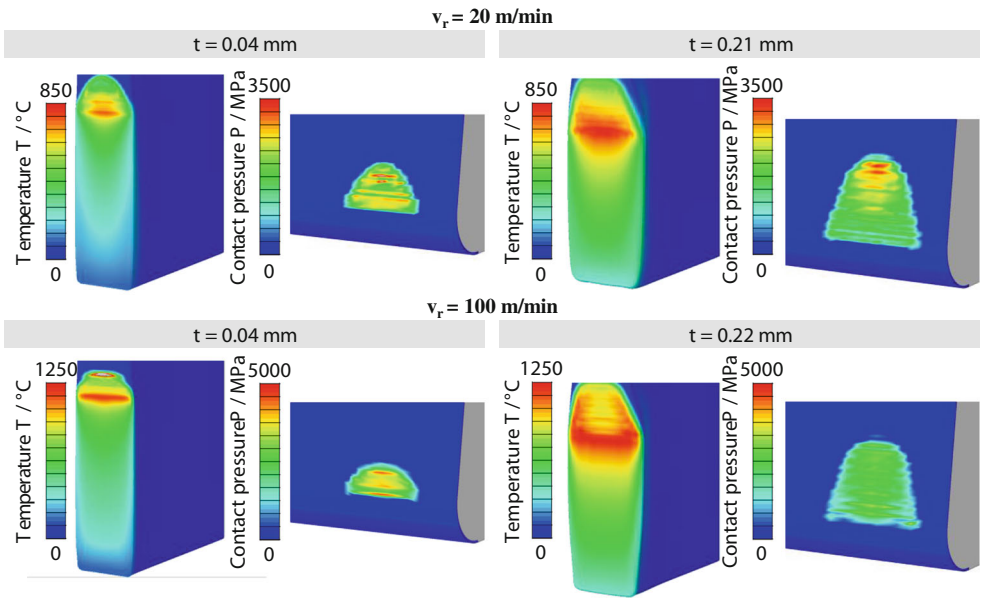

Fig. 14 The tool contact pressure and the contact temperature from the FEM simulations

the insertion leads to significant changes in the system behavior, and hence, to deviations in the measurement [12]. In the case of application of infrared thermography to measure the side face of the tool, the measured temperature is usually lower than the actual contact temperature [2]. Due to the difference between the local and measured contact temperature, the local contact temperature must be calibrated and estimated. It is also valid for the contact pressure, as the contact pressure was not uniformly distributed on the contact interface, as shown in Fig. 14. Hence, the mean contact pressure determined from the total process forces deviated from the maximum contact pressure.

It led to a systematic deviation between the experimental and numerical results with respect to the friction coefficient. The FEM simulations verified also the trend in Fig. 12 that the contact pressure decreased slightly with the rise of the depth of engagement (t) and increased significantly with the increase of the relative speed (v_r).

4 Conclusions

In this paper, the friction behavior between DA718, AISI1045 and cemented carbide tools was investigated under different relative speeds and process normal forces. Furthermore, an advanced friction model was proposed and validated according the experimental and numerical investigation. The following conclusions can be made from this research:

1. The apparent friction coefficients were dependent on the relative speeds and the process normal forces. A pure temperature- or speed-dependent friction model is not sufficient to describe the friction behavior.
2. The friction mechanisms including adhesion and deformation changed with the combination of workpiece and cutting tool materials. The workpiece deformation is the dominant friction mechanism that influences the friction coefficients for DA718 under cutting conditions.
3. A new friction model was proposed as a function of the relative speed (v_r), the measured contact temperature (T_m), and the mean contact pressure (p_m). With the proposed friction model, the FEM friction test is able to replicate the influence of the engagement depth and the relative speed on the friction coefficient.
4. The determined friction model showed that the friction coefficient increased with increasing temperature. One possible reason could be the increase of the internal friction with the increase of the temperature. However, more efforts should be made to study the influence of the temperature separately under cutting conditions.

The proposed friction model will be calibrated and implemented in FEM chip formation simulations in future work. Besides, the test bench should be improved to study the influence of the temperature on the friction behavior separately.

Funding information The study is supported by the German Research Foundation (DFG) for the funding of the depicted research within the project. The authors wish to thank the German Research Foundation (DFG) for funding the depicted research within the project.

References

1. Albrecht P (1960) New developments in the theory of the metal-cutting process: Part I. The ploughing process in metal cutting. J Eng Ind 82(4):348. https://doi.org/10.1115/1.3664242
2. Arrazola PJ, Aristimuno P, Soler D, Childs T (2015) Metal cutting experiments and modelling for improved determination of chip/tool contact temperature by infrared thermography. CIRP Ann 64(1):57–60. https://doi.org/10.1016/j.cirp.2015.04.061
3. Arrazola PJ, Özel T (2010) Investigations on the effects of friction modeling in finite element simulation of machining. Int J Mech Sci 52(1):31–42. https://doi.org/10.1016/j.ijmecsci.2009.10.001
4. Arrazola PJ, Özel T, Umbrello D, Davies M, Jawahir IS (2013) Recent advances in modelling of metal machining processes. CIRP Ann Manuf Technol 62(2):695–718. https://doi.org/10.1016/j.cirp.2013.05.006
5. Arrazola PJ, Ugarte D, Domínguez X (2008) A new approach for the friction identification during machining through the use of finite element modeling. Int J Mach Tools Manuf 48(2):173–183. https://doi.org/10.1016/j.ijmachtools.2007.08.022
6. Blanter MS (2007) Internal friction in metallic materials: a handbook Springer series in materials science, vol 90. Springer, Berlin and New York
7. Bobzin K, Brögelmann T, Kruppe NC, Hoffmann DC, Klocke F, Mattfeld P, Trauth D, Hild R (2018) Tribological studies on self-lubricating (cr,al)n+mo: S coatings at elevated temperature. Surf Coat Technol 353:282–291. https://doi.org/10.1016/j.surfcoat.2018.06.067
8. Bonnet C, Valiorgue F, Rech J, Claudin C, Hamdi H, Bergheau JM, Gilles P (2008) Identification of a friction model—application to the context of dry cutting of an AISI 316L austenitic stainless steel with a TiN coated carbide tool. Int J Mach Tools Manuf 48(11):1211–1223. https://doi.org/10.1016/j.ijmachtools.2008.03.011
9. Brocail J, Watremez M, Dubar L (2010) Identification of a friction model for modelling of orthogonal cutting. Int J Mach Tools Manuf 50(9):807–814. https://doi.org/10.1016/j.ijmachtools.2010.05.003
10. Claudin C, Rech J, Grzesik W (2008) Development of a new tribometer to identify the effects of coatings and lubricants during machining processes 2008
11. Courbon C, Mabrouki T, Rech J, Mazuyer D, D'Eramo E (2013) On the existence of a thermal contact resistance at the tool-chip interface in dry cutting of AISI 1045: formation mechanisms and influence on the cutting process. Appl Therm Eng 50(1):1311–1325. https://doi.org/10.1016/j.applthermaleng.2012.06.047
12. Davies MA, Ueda T, M'Saoubi R, Mullany B, Cooke AL (2007) On the measurement of temperature in material removal processes. CIRP Ann Manuf Technol 56(2):581–604. https://doi.org/10.1016/j.cirp.2007.10.009
13. Egaña A, Rech J, Arrazola PJ (2012) Characterization of friction and heat partition coefficients during machining of a TiAl6V4 titanium alloy and a cemented carbide. Tribol Trans 55(5):665–676. https://doi.org/10.1080/10402004.2012.692007

14. Fukuhara M, Sanpei A (1993) Elastic moduli and internal frictions of Inconel 718 and ti-6Al-4V as a function of temperature. J Mater Sci Lett 12(14):1122–1124. https://doi.org/10.1007/BF00420541
15. Grzesik W (1999) Experimental investigation of the influence of adhesion on the frictional conditions in the cutting process. Tribology Int 32(1):15–23
16. Ishikawa K, Ishikawa K (1982) Guide to quality control, vol. 2 Asian Productivity Organization Tokyo
17. Klocke F (2011) Manufacturing process. RWTH edition. Springer, Berlin
18. Klocke F, Döbbeler B, Peng B, Schneider S (2018) Tool-based inverse determination of material model of direct aged alloy 718 for FEM cutting simulation. Procedia CIRP 77:54–57. https://doi.org/10.1016/j.procir.2018.08.211
19. Klocke F, Trauth D, Shirobokov A, Mattfeld P (2015) FE-Analysis and in situ visualization of pressure-, slip-rate-, and temperature-dependent coefficients of friction for advanced sheet metal forming: development of a novel coupled user subroutine for shell and continuum discretization. Int J Advan Manuf Technol 81(1-4):397–410. https://doi.org/10.1007/s00170-015-7184-1
20. Melkote SN, Grzesik W, Outeiro J, Rech J, Schulze V, Attia H, Arrazola PJ, M'Saoubi R, Saldana C (2017) Advances in material and friction data for modelling of metal machining. CIRP Ann 66(2):731–754. https://doi.org/10.1016/j.cirp.2017.05.002
21. Merchant ME (1945) Mechanics of the metal cutting process. II. Plasticity conditions in orthogonal cutting. J Appl Phys 16(6):318–324. https://doi.org/10.1063/1.1707596
22. Moufki A, Molinari A, Dudzinski D (1998) Modelling of orthogonal cutting with a temperature dependent friction law. J Mech Phys Solids 46(10):2103–2138. https://doi.org/10.1016/S0022-5096(98)00032-5
23. Neugebauer R, Bouzakis KD, Denkena B, Klocke F, Sterzing A, Tekkaya AE, Wertheim R (2011) Velocity effects in metal forming and machining processes. CIRP Ann 60(2):627–650. https://doi.org/10.1016/j.cirp.2011.05.001
24. Oxley PLB (1963) Rate of strain effect in metal cutting. J Eng Indust 85(4):335. https://doi.org/10.1115/1.3669884
25. Özel T (2006) The influence of friction models on finite element simulations of machining. Int J Mach Tools Manuf 46(5):518–530. https://doi.org/10.1016/j.ijmachtools.2005.07.001
26. Puls H, Klocke F, Lung D (2014) Experimental investigation on friction under metal cutting conditions. Wear 310(1-2):63–71. https://doi.org/10.1016/j.wear.2013.12.020
27. Rech J, Arrazola PJ, Claudin C, Courbon C, Pusavec F, Kopac J (2013) Characterisation of friction and heat partition coefficients at the tool-work material interface in cutting. CIRP Ann Manuf Technol 62(1):79–82. https://doi.org/10.1016/j.cirp.2013.03.099
28. Smolenicki D, Boos J, Kuster F, Roelofs H, Wyen CF (2014) In-process measurement of friction coefficient in orthogonal cutting. CIRP Ann 63(1):97–100. https://doi.org/10.1016/j.cirp.2014.03.083
29. Zemzemi F, Rech J, Ben Salem W, Dogui A, Kapsa P (2009) Identification of a friction model at tool/chip/workpiece interfaces in dry machining of AISI4142 treated steels. J Mater Process Technol 209(8):3978–3990. https://doi.org/10.1016/j.jmatprotec.2008.09.019
30. Zhou F (2014) A new analytical tool-chip friction model in dry cutting. Int J Advan Manuf Technol 70(1-4):309–319. https://doi.org/10.1007/s00170-013-5271-8